

# Fluctuations of pion flow harmonics and HBT correlation functions in ultrarelativistic heavy ion collisions

Ying Hu<sup>1</sup>, Wei-Ning Zhang<sup>1,2\*</sup>, Yan-Yu Ren<sup>2</sup>

<sup>1</sup>*School of Physics and Optoelectronic Technology,*

*Dalian University of Technology, Dalian, Liaoning 116024, China*

<sup>2</sup>*Department of Physics, Harbin Institute of Technology, Harbin, Heilongjiang 150006, China*

We investigate the fluctuations of pion elliptic flow, triangular flow, and Hanbury-Brown-Twiss (HBT) correlation functions for the hydrodynamic sources with fluctuating initial conditions in the heavy ion collisions of Au-Au at  $\sqrt{s_{NN}} = 200$  GeV and Pb-Pb at  $\sqrt{s_{NN}} = 2.76$  TeV. A method based on sub-event collection analysis is used to detect these fluctuations in ultrarelativistic heavy ion collisions. We investigate the relationship between source initial granular inhomogeneity and the fluctuations of the flow harmonics and HBT correlation functions. Our study indicate that the fluctuations of triangle flow are very sensitive to the source initial granularity.

PACS numbers: 25.75.-q, 25.75.Gz

It is well known that the initial systems created in the heavy ion collisions at the highest energy of the Relativistic Heavy Ion Collider (RHIC) and the energy of the Large Hadron Collider (LHC) are not uniform in space, and there are event-by-event fluctuations of the system initial quantities [1]. The studies of the propagation of the fluctuating initial conditions (FIC) through system evolution and their influence on final particle observables are recently very interesting issues in high energy heavy ion collisions [1].

Elliptic flow and two-particle Hanbury-Brown-Twiss (HBT) correlation functions are important observables in high energy heavy ion collisions. They reflects the transverse (perpendicular to beam direction) anisotropic pressure property and space-time structure of the particle-emitting sources, respectively. In ultrarelativistic heavy ion collisions, the spectators depart from the reaction region quickly after collision, and a very hot and dense fireball is created in the mid-rapidity region. For uniform systems of the fireball the odd-order azimuthal flow harmonics are expected to be zero. However, recent investigations indicate that the initial density fluctuations of the system may lead to nonzero triangle flow, and thus inspires the investigations of azimuthal triangle flow and even higher-order flow harmonics [2–9]. On event-by-event basis, the particle-emitting sources associated with the FIC are bumpy and inhomogeneous [5, 10–13]. This inhomogeneous structure may bring the fluctuations of final particle observables. It is of interest to detect the fluctuations of elliptic flow, triangle flow, and HBT correlation functions in ultrarelativistic heavy ion collisions, and investigate the relationship between the final observable fluctuations and the initial inhomogeneity of the sources.

In this work, we use the Heavy Ion Jet Interaction Generator (HIJING) [14] to generate the FIC of the

particle-emitting sources for the heavy ion collisions of Au-Au at  $\sqrt{s_{NN}} = 200$  GeV at the RHIC and Pb-Pb at  $\sqrt{s_{NN}} = 2.76$  TeV at the LHC. The system evolution is described by relativistic hydrodynamics with the equation of state of s95p-PCE, which combines the hadron resonance gas at low temperature and the lattice QCD results at high temperature [15]. Under the assumption of Bjorken longitudinal boost invariance [16], the hydrodynamics in (3+1) dimensions reduces to (2+1) dimensions. In this case we need only to solve the transverse ( $xy$ -plane) equations of motion, and the hydrodynamic solutions at  $z \neq 0$  can be obtained by the longitudinal boost invariance hypothesis [10, 17, 18]. Assuming that the initial local equilibrium system is formed at time  $\tau_0$ , we construct the initial energy density at  $z = 0$ , by using the AMPT code [19] in which the HIJING is used for generating the initial conditions, for the hydrodynamic evolving source with [10, 20]

$$\varepsilon(\tau_0, x, y; z = 0) = K \sum_{\alpha} \frac{p_{\perp\alpha}}{\tau_0} \frac{1}{2\pi\sigma_0^2} \times \exp \left\{ -\frac{[x - x_{\alpha}(\tau_0)]^2 + [y - y_{\alpha}(\tau_0)]^2}{2\pi\sigma_0^2} \right\}. \quad (1)$$

Here  $p_{\perp\alpha}$  is the transverse momentum of parton  $\alpha$ ,  $x_{\alpha}(\tau_0)$  and  $y_{\alpha}(\tau_0)$  are the transverse coordinates of the parton at  $\tau_0$ ,  $\sigma_0$  is a transverse width parameter, and  $K$  is a scale factor which can be adjusted to fit the experimental data of produced hadrons [20].

In Fig. 1 [(a1)– (c1)] and [(d1)– (f1)], we show the transverse distributions of the source initial energy density at  $z = 0$  for the Au-Au and Pb-Pb collisions at the RHIC and LHC energies, respectively. The impact parameter  $b$  for both the RHIC and LHC heavy ion collisions is 4 fm, and the unit of energy density is GeV/fm<sup>3</sup>. The energy density evolutions with time after  $\tau_0$  are shown in the panels [(a2)– (a4)], [(b2)– (b4)], [(c2)– (c4)], [(d2)– (d4)], [(e2)– (e4)], [(f2)– (f4)], respectively. One can see from the panels [(a1)– (c1)] and [(d1)– (f1)] that the initial energy density is fluctuated. There are hot spots and cold valleys in the systems. We call this in-

\*Email: wnzhang@dlut.edu.cn

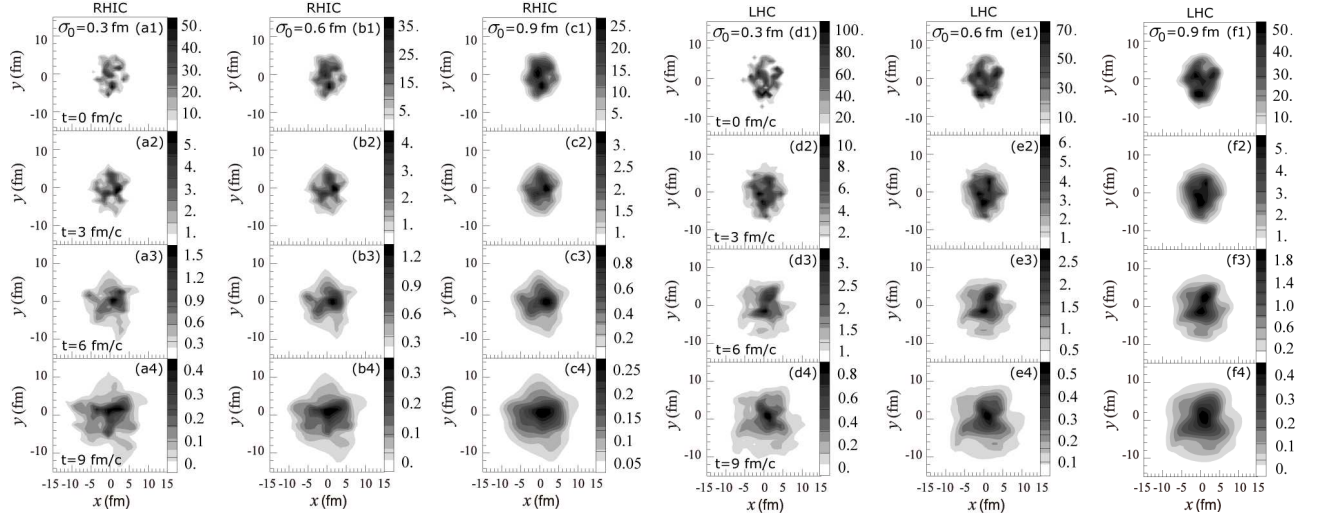


FIG. 1: The transverse distributions of energy density at  $z = 0$  for the Au-Au collisions at  $\sqrt{s_{NN}} = 200$  GeV at the RHIC and the Pb-Pb collisions at  $\sqrt{s_{NN}} = 2.76$  TeV at the LHC. The impact parameter  $b$  for both the RHIC and LHC heavy ion collisions is 4 fm, and  $\sigma_0$  values are 0.3, 0.6, and 0.9 fm. The panels [(a1)– (f1)], [(a2)– (f2)], [(a3)– (f3)], [(a4)– (f4)] are for the evolution time after  $\tau_0$ ,  $t = 0, 3, 6,$  and  $9$  fm/c, respectively. The unit of energy density is  $\text{GeV}/\text{fm}^3$ .

homogeneity as granular inhomogeneous structure of hot spot. The maximum of the energy density of spot decreases with impact parameter  $b$ , and the number of the spots decreases with the value of  $\sigma_0$ . From the panels of time greater than zero one can see that the late sources are still inhomogeneous due to the initial fluctuations. In Fig. 2 (a) and (b), we show the pion transverse momentum spectra calculated by the hydrodynamics with the FIC (solid lines) and the smoothed initial conditions (SIC) which are obtained by averaging the FIC over 100 events, for the Au-Au and Pb-Pb collisions at the RHIC and LHC energies, respectively. The circle, up-triangle, and square symbols are the experimental data [21, 22]. In the hydrodynamic calculations, we take the same cuts for particle rapidity  $y$  as in the experimental analyses [21, 22]. The freeze out temperature is taken to be 130 MeV, and the parameter  $\sigma_0$  is 0.6 fm. For the centralities 0–5%, 10–20%, and mini bias, the regions of impact parameter are taken to be 0–2.3, 4.2–5.9, and 0–10.2 fm, respectively [23]. It can be seen that the hydrodynamic results with the FIC are consistent with the experimental data. They are higher than the hydrodynamic results with the SIC at large  $p_T$ .

In high energy heavy ion collisions, the invariant momentum distribution of final particles can be written in the form of a Fourier series [24, 25],

$$E \frac{d^3 N}{d^3 p} = \frac{1}{2\pi} \frac{d^2 N}{p_T dp_T dy} \left[ 1 + \sum_n 2v_n \cos(n\phi - n\Psi_R) \right], \quad (2)$$

where  $\phi$  and  $\Psi_R$  are the azimuthal angles of the measured particle and event reaction plane. The first term on the right side of Eq. (2) is the transverse momentum spectrum, and the coefficients in the summation,  $v_n = \langle \cos[n(\phi - \Psi_R)] \rangle$ , are the azimuthal  $n$ th-order flow harmonics, where the average  $\langle \dots \rangle$  is over particles and

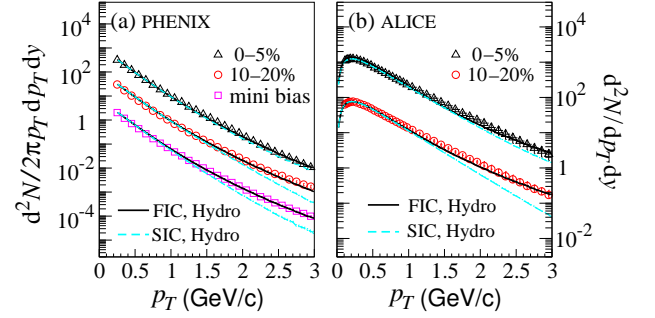


FIG. 2: (Color online) The pion transverse momentum spectra for the Au-Au collisions at the RHIC energy  $\sqrt{s_{NN}} = 200$  GeV [panel (a)] and the Pb-Pb collisions at the LHC energy  $\sqrt{s_{NN}} = 2.76$  TeV [panel (b)]. The solid lines are the hydrodynamic results with the FIC, and the dashed lines are the hydrodynamic results with the SIC which are obtained by averaging the FIC over 100 events. The circle, up-triangle, and square symbols are the experimental data [21, 22].

events. In experimental data analyses, the reaction plane is usually replaced by the event plane which is determined with the measured particles in an event [26, 27]. An alternative technique in flow analyses is the measurement of the two-particle cumulant of azimuthal correlations,  $[v_n\{2\}]^2 = \langle \cos[n(\phi_1 - \phi_2)] \rangle$  [28, 29], which avoids the uncertainty in estimating reaction plane. In this letter, we calculate the integrated and  $p_T$ -differential flow harmonics with the two-particle cumulant method [28] as,

$$v'_n\{2\} = \left[ \frac{N_n\{2\}}{N_{\text{pair}}} \right]^{\frac{1}{2}} = \left\{ \frac{1}{N_{\text{pair}}} \sum_{\alpha=1}^{N_{\text{evt}}} \sum_{i,j,\neq}^{N_{\text{part}}} \cos n(\phi_i - \phi_j) \right\}^{\frac{1}{2}}, \quad (3)$$

$$v_n\{2\}(p_T) = \frac{N_n\{2\}(p_T)}{N_{\text{pair}}(p_T)} \frac{1}{v'_n\{2\}}, \quad (4)$$

where  $N_{\text{pair}}$  is the total number of particle pairs in the  $N_{\text{evt}}$  events with the particle multiplicity  $N_{\text{part}}$ ,  $N_{\text{pair}}(p_T)$  and  $N_n\{2\}(p_T)$  are the counting numbers of the particle pairs in the  $p_T$  bins with the weights 1 and  $\cos[n(\phi_i - \phi_j)]$ , respectively.

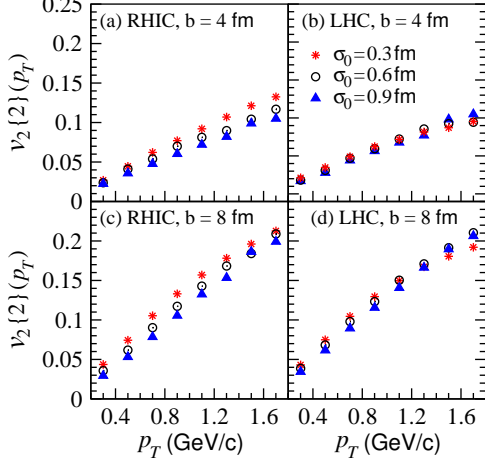


FIG. 3: (Color online) The pion elliptic flow of the hydrodynamic sources for the Au-Au collisions at the RHIC energy  $\sqrt{s_{NN}} = 200$  GeV and the Pb-Pb collisions at the LHC energy  $\sqrt{s_{NN}} = 2.76$  TeV with impact parameter  $b = 4$  and 8 fm. The symbols of stars, circles, and upward triangles are for the parameter  $\sigma_0 = 0.3, 0.6$  and 0.9 fm, respectively.

In Fig. 3 we plot the pion  $p_T$ -differential elliptic flow of the hydrodynamic sources for Au-Au collisions at the RHIC energy  $\sqrt{s_{NN}} = 200$  GeV and Pb-Pb collisions at the LHC energy  $\sqrt{s_{NN}} = 2.76$  TeV with impact parameter  $b = 4$  and 8 fm. In our calculations, the number of events  $N_{\text{evt}}$  is six thousand and the particle-pair number for each event  $N_{\text{pair}}$  is  $10^6$ . One can see that the values of elliptic flow decrease with parameter  $\sigma_0$  for the RHIC collisions, and are almost independent of it for the LHC collisions. In Fig. 4 the dashed lines show the elliptic flow of the sub-event collections with the 100 events for the RHIC and LHC heavy ion collisions. The solid lines are the results averaged over sixty the sub-event collections. The error bars are the statistics errors,

$$\begin{aligned} \Delta[v_n\{2\}(p_T)] &= v_n\{2\}(p_T) \left[ \frac{1}{\sqrt{N_n\{2\}(p_T)}} \right. \\ &\quad \left. + \frac{1}{\sqrt{N_{\text{pair}}(p_T)}} + \frac{1}{2\sqrt{N_n\{2\}}} + \frac{1}{2\sqrt{N_{\text{pair}}}} \right] \\ &\approx v_n\{2\}(p_T) \left[ \frac{1}{\sqrt{N_n\{2\}(p_T)}} + \frac{1}{\sqrt{N_{\text{pair}}(p_T)}} \right]. \end{aligned} \quad (5)$$

One can see from Fig. 4 that the flow calculated with the 100 events are still with great fluctuations, which are larger than the statistics errors. The fluctuations reflect the intrinsic properties of the sources.

As is well known the azimuthal flow harmonics are re-

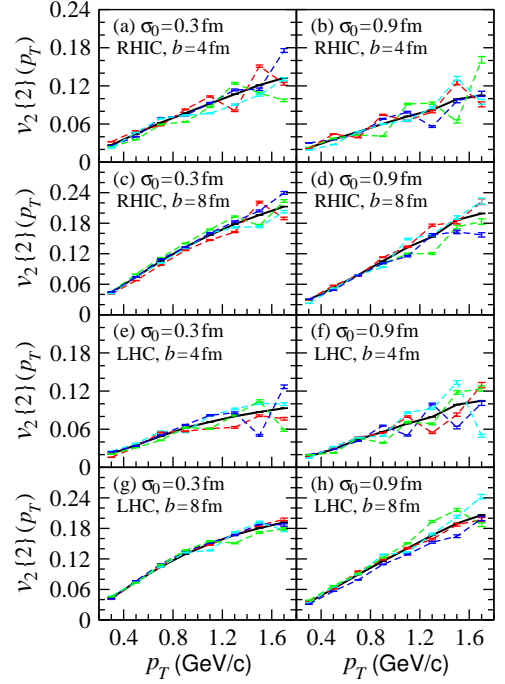


FIG. 4: (Color online) The pion elliptic flow of the sub-event collections with the 100 events (dashed lines) for the RHIC Au-Au collisions and the LHC Pb-Pb collisions with impact parameter  $b = 4$  and 8 fm. For each event the particle pair number is  $10^6$ . The solid lines are the averaged results over the sixty collections.

lated to the initial eccentricities of the source,

$$\varepsilon_n = \frac{\sqrt{\langle \rho^2 \cos(n\phi') \rangle^2 + \langle \rho^2 \sin(n\phi') \rangle^2}}{\langle \rho^2 \rangle}, \quad (6)$$

where  $\phi'$  is the azimuthal angle related to the reaction plane ( $xz$  plane) and  $\rho$  is the transverse coordinate of source point. In order to have a approximate understanding for the elliptic flow of the FIC sources, we use a simple source distribution of separated droplets to calculate the eccentricity  $\varepsilon_2$ . The single-event transverse source distribution is given by [30, 31]

$$D(\boldsymbol{\rho}) = \frac{1}{N_d(2\pi a^2)} \sum_{i=1}^{N_d} \exp \left[ -\frac{(\boldsymbol{\rho} - \mathbf{R}_{\perp i})^2}{2a^2} \right], \quad (7)$$

where  $N_d$  is the number of droplet,  $\mathbf{R}_{\perp i} = (\mathbf{X}_i, \mathbf{Y}_i)$  are the transverse coordinates of droplet centers, and  $a$  is the standard deviation of Gaussian distribution. So, for a single event we have

$$\begin{aligned} \langle \rho^2 \cos(2\phi') \rangle &= \frac{1}{N_d} \sum_{i=1}^{N_d} (Y_i^2 - X_i^2), \\ \langle \rho^2 \sin(2\phi') \rangle &= \frac{1}{N_d} \sum_{i=1}^{N_d} 2X_i Y_i, \\ \langle \rho^2 \rangle &= \frac{1}{N_d} \sum_{i=1}^{N_d} (2a^2 + X_i^2 + Y_i^2). \end{aligned} \quad (8)$$

Further, assume that the central coordinates of the droplets obey the Gaussian distribution,  $P(X_i, Y_i) \sim \exp(-X_i^2/2\mathcal{R}_x^2 - Y_i^2/2\mathcal{R}_y^2)$ . By substituting the summation  $\frac{1}{N_d} \sum_i$  in Eq. (8) with  $\int dX_i dY_i P(X_i, Y_i)$  and finishing the integration, we get

$$\begin{aligned} \langle \rho^2 \cos(2\phi') \rangle &= \mathcal{R}_y^2 - \mathcal{R}_x^2, & \langle \rho^2 \sin(2\phi') \rangle &= 0, \\ \langle \rho^2 \rangle &= 2a^2 + \mathcal{R}_x^2 + \mathcal{R}_y^2, \end{aligned} \quad (9)$$

and the  $\varepsilon_2$  for a huge number of events is

$$\varepsilon_2 = \frac{\mathcal{R}_y^2 - \mathcal{R}_x^2}{2a^2 + \mathcal{R}_x^2 + \mathcal{R}_y^2}. \quad (10)$$

The eccentricity decreases with the droplet radius  $a$  and the variation of  $\varepsilon_2$  with  $a$  becomes light when  $\mathcal{R}_x$  and  $\mathcal{R}_y$  are large. These conclusions are consistent with the results in Fig. 3, where  $\sigma_0 \sim a$ . In Eq. (8),  $N_d$ ,  $X_i$ , and  $Y_i$  vary chaotically event-by-event. It leads to the fluctuations of the values of elliptic flow calculated with single and finite number events as shown in Fig. 4.

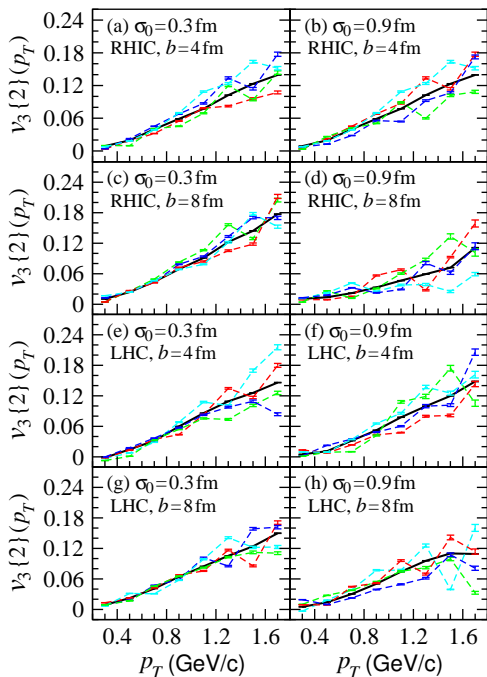


FIG. 5: (Color online) The pion triangle flow of the sub-event collections with the 100 events (dashed lines) for the RHIC Au-Au collisions and the LHC Pb-Pb collisions with impact parameter  $b = 4$  and 8 fm. For each event the particle pair number is  $10^6$ . The solid lines are the averaged results over the sixty collections.

In Fig. 5 the dashed lines show the triangle flow for the sub-event collections as in Fig. 4. The solid lines are the results averaged over sixty the sub-event collections. As compared to the results of elliptic flow in Fig. 4, the fluctuations of triangle flow are larger. The values of triangle flow are related to the initial third-order

TABLE I: The eccentricities, transverse radius, and granularity parameter of the initial sources for the RHIC and LHC collisions with different  $b$  and  $\sigma_0$ .

	$b$ (fm)	$\sigma_0$ (fm)	$\varepsilon_2$	$\varepsilon_3$	$\langle \rho_0 \rangle$ (fm)	$L_\xi$ (fm)
RHIC	4.0	0.3	0.189	0.091	3.285	6.80
	4.0	0.6	0.183	0.085	3.341	7.67
	4.0	0.9	0.172	0.076	3.433	9.47
RHIC	8.0	0.3	0.375	0.143	2.600	5.49
	8.0	0.6	0.356	0.129	2.684	6.71
	8.0	0.9	0.322	0.110	2.808	9.53
LHC	4.0	0.3	0.172	0.076	3.649	7.50
	4.0	0.6	0.167	0.075	3.698	8.27
	4.0	0.9	0.165	0.065	3.788	9.79
LHC	8.0	0.3	0.367	0.112	2.904	6.08
	8.0	0.6	0.350	0.105	2.984	7.11
	8.0	0.9	0.325	0.092	3.093	9.35

eccentricity  $\varepsilon_3$ , which may become non-zero due to the granular inhomogeneous structure of the initial sources. Because involving elliptic integrations, we cannot obtain an analytic expression of  $\varepsilon_3$  even for the simple droplet model. In Table I we list the values of  $\varepsilon_2$  and  $\varepsilon_3$  calculated with the initial energy density (see the top panels in Fig. 1) for the sources of the RHIC and LHC collisions with the different values of  $b$  and  $\sigma_0$ . The values of  $\varepsilon_2$  and  $\varepsilon_3$  increase with impact parameter  $b$  and decrease with  $\sigma_0$ . Comparing the results of the averaged triangle flow in Figs. 5 (b) and 5 (d) for the different  $b$  and the same  $\sigma_0$ , we find they are contradictory to the corresponding  $\varepsilon_3$  values in Table I. It indicates there are other effects on the triangle flow values for different impact parameter.

To reveal the relationship between the fluctuations of the elliptic and triangle flows of the sub-event collections and the initial source granular inhomogeneity, we introduce the granularity length of the initial source as the product of the initial transverse radius of source  $\mathcal{R}_\perp$  and the granularity parameter  $\xi$  [30],

$$L_\xi = \mathcal{R}_\perp \xi = \mathcal{R}_\perp \frac{(\mathcal{R}_\perp / \sigma_0)^2}{N_d - 2} \approx \frac{2\langle \rho_0 \rangle^3}{\langle \rho_0 \rangle^2 - 4\sigma_0^2}. \quad (11)$$

Here, we replace  $\mathcal{R}_\perp$  approximately with the average transverse coordinate of the initial source  $\langle \rho_0 \rangle$ , and replace  $N_d$  approximately with  $\frac{1}{2}(\langle \rho_0 \rangle / \sigma_0)^2$ , considering the same numbers of hot spots and cold valleys in the initial source. For given source and droplet radii, the granularity length increase when the droplet number decreases, and reaches to the maximum when  $N_d = 2$ . On the other hand, the source with many small droplets will be more like a continued source and has small granularity. In the right two columns of Table I, we presents the  $\langle \rho_0 \rangle$  and  $L_\xi$  values of the initial sources. The values of  $\langle \rho_0 \rangle$  decrease with impact parameter  $b$  and increase slightly with  $\sigma_0$  for fixed  $b$ . The values of  $\langle \rho_0 \rangle$  are larger for the

LHC collisions as compared to the corresponding results for the RHIC collisions. The values of  $L_\xi$  increase with  $\sigma_0$  because the droplet number decreases with  $\sigma_0$ . In most case, the values of  $L_\xi$  for smaller  $b$  are larger than those for larger  $b$  because the initial sources are larger for smaller  $b$ . For the same reason, the values of  $L_\xi$  for the LHC sources are larger than the corresponding results for the RHIC sources. However, we observe an exception for the largest  $b$  and  $\sigma_0$  in Table I for the RHIC source. The large value of  $L_\xi$  for  $b = 8$  fm and  $\sigma_0 = 0.9$  fm is because that the droplet number is very small in this case. It will be see that for the RHIC or LHC sources the large granularity length corresponds to the large fluctuations of the elliptic and triangle flows of sub-event collections.

To describe the flow harmonic fluctuations of sub-event collections, we introduce the distribution  $dN/df$  of the differences,

$$f_{vn} = |v_n^{(i)}\{2\} - v_n^{(j)}\{2\}|, \quad (12)$$

where the superscripts indicate the sub-event collections. Unlike some cumulate quantities which smooth out the fluctuations, the distribution  $dN/df$  becomes wide for the variables with large fluctuations [12, 32]. Because the event numbers of collisions are very huge, the statistics of the distribution is unlimited in principle.

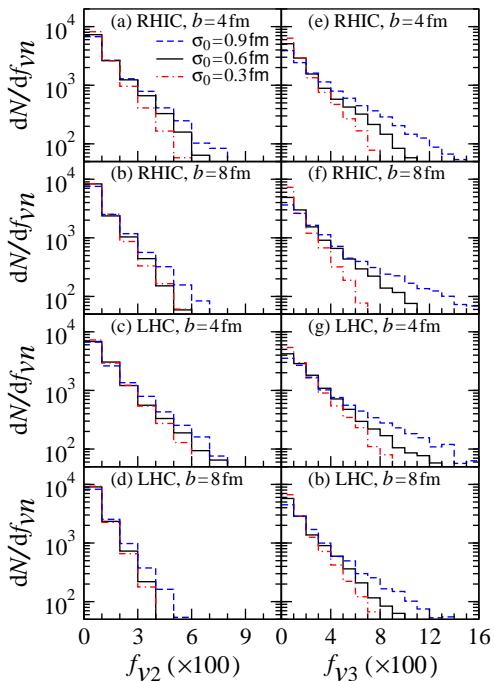


FIG. 6: (Color online) The distributions  $dN/df_{vn}$  for the RHIC Au-Au collisions and the LHC Pb-Pb collisions with different impact parameter  $b$  and parameter  $\sigma_0$ .

In Fig. 6, we plot the distributions  $dN/df_{vn}$  for the RHIC and LHC sources with different impact parameter  $b$  and parameter  $\sigma_0$ . The widths of the distributions increase with  $\sigma_0$ , and in most case the widths decrease

with  $b$  for fixed  $\sigma_0$ . The larger the fluctuations, the wider the distribution  $dN/df$  is. For the sources at the RHIC or LHC energies, the distribution widths (thus the fluctuations) are obviously proportional to the granularity length  $L_\xi$ , especially the triangle flow results. These indicate that the fluctuations of the flow harmonics are related to the source initial granular inhomogeneity, and the distribution width of triangle flow is sensitive to the source granularity. Comparing both the  $dN/df_{vn}$  distributions in Fig. 6 and the  $L_\xi$  values in Table I for the RHIC and LHC sources with the same  $b$  and  $\sigma_0$ , we observe a contradiction between the distribution widths and the  $L_\xi$  values. For instance, the  $L_\xi$  value for the LHC source with  $b = 8$  fm and  $\sigma_0 = 0.6$  fm is larger than that for the RHIC source, but the corresponding distribution width for the LHC source is smaller. It indicates that there are other dynamical effects which are different in the collisions at the RHIC and LHC energies.

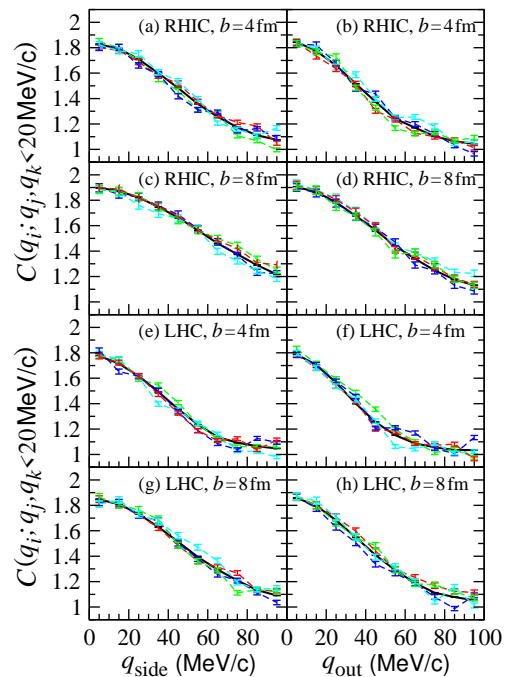


FIG. 7: (Color online) The HBT correlation functions of the sub-event collections with the ten events (dashed lines) for the RHIC Au-Au collisions and the LHC Pb-Pb collisions with different impact parameter  $b$  and  $\sigma_0 = 0.6$  fm. The solid lines are the averaged results over the six hundred collections.

For the event-by-event inhomogeneous sources, the single- or several-event HBT correlation functions are fluctuated [12, 31–33]. In Fig. 7 we plot the two-pion HBT correlation functions of the sub-event collections with the ten events (dashed lines) for the RHIC Au-Au collisions and the LHC Pb-Pb collisions with different impact parameter  $b$  and  $\sigma_0 = 0.6$  fm. Here,  $q_{\text{side}}$  and  $q_{\text{out}}$  are the relative transverse momenta of the pion pair in the “side” and “out” directions [34, 35]. The solid lines are the averaged results over the six hundred collections.

We observe the fluctuations of the HBT correlations for the sub-event collections, and they are smoothed out in the average results.

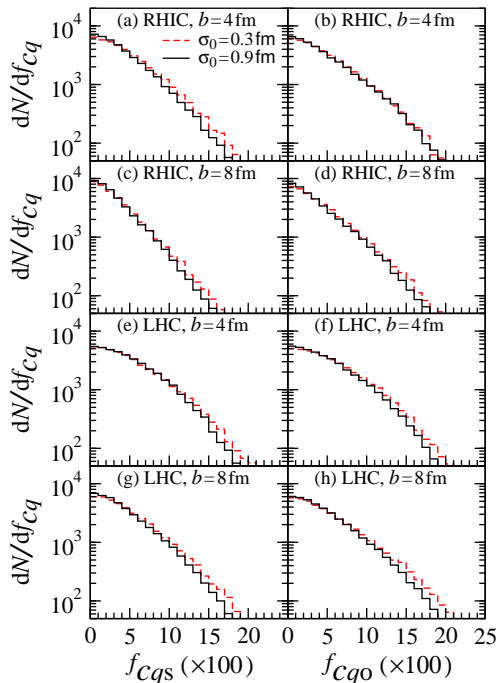


FIG. 8: (Color online) The distributions  $dN/df_C$  for the RHIC and LHC sources with different impact parameter  $b$  and  $\sigma_0$ .

In Fig. 8 we show the distributions  $dN/df_C$  for the HBT correlation functions  $C(q_{\text{side}})$  and  $C(q_{\text{out}})$  for the RHIC and LHC sources with different impact parameter  $b$  and  $\sigma_0$ . We find the distributions are insensitive to  $\sigma_0$ , although they may become wider as compared to the distributions for the source with smoothed initial conditions [12, 33]. Unlike elliptic flow and triangle flow, HBT correlation functions reflect more the source freeze-out geometry and dynamics than the initial details of the sources.

In Fig. 9 we show the root-mean-square  $f_{\text{rms}}$  of the distributions  $dN/df$  for elliptic flow, triangle flow, and HBT correlation functions as functions of the granularity length of the initial source. It can be seen that the root-mean-square values of the flow harmonics increase with  $L_\xi$ , and the root-mean-square values of HBT correlation functions are almost independent of  $L_\xi$ . The root-mean-square values of triangle flow are very sensitive to the initial granularity of the sources.

In summary, we investigate the fluctuations of pion elliptic flow, triangular flow, and HBT correlation func-

tions for the hydrodynamic sources with fluctuating initial conditions in the heavy ion collisions of Au-Au at  $\sqrt{s_{NN}} = 200$  GeV and Pb-Pb at  $\sqrt{s_{NN}} = 2.76$  TeV. We introduce a granularity length to describe the initial granular inhomogeneity of the sources and investigate its relationship with the fluctuations of the pion flow harmonics

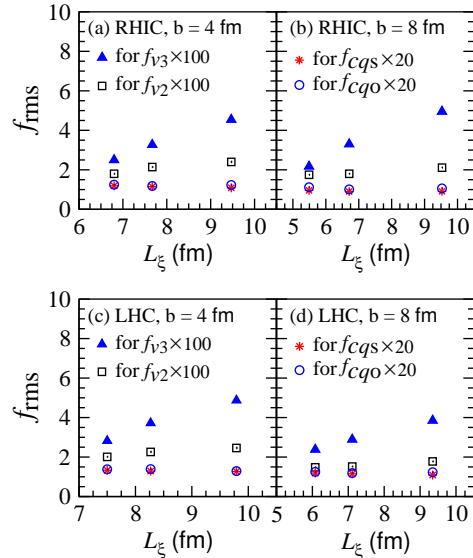


FIG. 9: (Color online) The root-mean-square  $f_{\text{rms}}$  of the distributions  $dN/df$  for the elliptic flow, triangle flow, and HBT correlation functions as functions of  $L_\xi$ , for the RHIC and LHC sources with the impact parameter  $b = 4$  and  $8$  fm.

and HBT correlation functions of sub-event collections. These investigations indicate that the fluctuations of the elliptic flow, triangle flow, and HBT correlation functions can be detected by the distributions  $dN/df$  of the absolute deviations  $f$  of the observable values between different sub-event collections. The width of the fluctuation distribution and the root-mean-square  $f_{\text{rms}}$  of triangle flow are very sensitive to the source initial granularity. They are hopeful observables for probing the details of the initial sources in ultrarelativistic heavy ion collisions.

### Acknowledgments

We thank Drs. Longgan Pang and Luan Cheng for helpful discussions. This work is supported by the National Natural Science Foundation of China under Contract No. 11275037.

[1] For a recent review see, A. Adare, M. Luzum and H. Petersen, Summary of the major findings and discussions of

the workshop "Initial State Fluctuations and Final State Correlations", held at ECT\* in Trento in July, 2012,

- arXiv:1212.5388; Phys. Scripta 87 (2013) 048001.
- [2] B. Alver, G. Roland, Phys. Rev. C **81** (2010) 054905.
- [3] B. Alver, C. Gombeaud, M. Luzum, J. Y. Ollitrault, Phys. Rev. C **82** (2010) 034913.
- [4] P. Staig, E. Shuryak, Phys. Rev. C **84** (2011) 034908.
- [5] B. Schenke, S. Jeon, C. Gale, Phys. Rev. Lett. **106** (2011) 042301; *ibid.* Phys. Rev. C **85** (2012) 024901.
- [6] K. Aamodt *et al.* (ALICE Collaboration), Phys. Rev. Lett. **107** (2011) 032301.
- [7] A. Adare *et al.* (PHENIX Collaboration), Phys. Rev. Lett. **107** (2011) 252301.
- [8] G. Ada *et al.* (ATLAS Collaboration), Phys. Rev. C **86** (2012) 014907.
- [9] C. Gale, S. Jeon, B. Schenke, P. Tribedy, R. Venugopalan, Phys. Rev. Lett. **110** (2013) 012302.
- [10] M. Gyulassy, D. H. Rischke, B. Zhang, Nucl. Phys. **613** (1997) 397.
- [11] T. Osada, C.E. Aguiar, Y. Hama, and T. Kodama, in Proc. of the 6th RANP Workshop, Eds. T. Kodama *et al.*, World Scientific, Singapore (2001), P. 174 [nucl-th/0102011].
- [12] Y. Y. Ren, W. N. Zhang, J. L. Liu, Phys. Lett. B **669** (2008) 317.
- [13] K. Werner, Iu. Karpenko, T. Pierog, M. Bleicher, and K. Mikhailov, Phys. Rev. C **82** (2010) 044904.
- [14] X. N. Wang, M. Gyulassy, Phys. Rev. D **44** (1991) 3501; M. Gyulassy, X. N. Wang, Comp. Phys. Commun. **83** (1994) 307.
- [15] C. Shen, U. Heinz, P. Huovinen, H. C. Song, Phys. Rev. C **82** (2010) 054904.
- [16] J. D. Bjorken, Phys. Rev. D **27** (1983) 140.
- [17] G. Baym, B. L. Friman, J. P. Blazot, M. Soyeur, W. Czyż, Nucl. Phys. A **407** (1983) 397.
- [18] Y. Hu, K. X. Feng, W. N. Zhang, Chin. Phys. C **38** (2014) 044102.
- [19] Z. W. Lin, C. M. Ko, B. A. Li, B. Zhang, S. Pal, Phys. Rev. C **72** (2005) 064901.
- [20] L. G. Pang, Q. Wang, X. N. Wang, Phys. Rev. C **86** (2012) 024911.
- [21] S. S. Adler *et al.* (PHENIX Collaboration), Phys. Rev. C **69** (2004) 034909.
- [22] R. Pughenella (for ALICE Collaboration), Acta. Phys. Pol. B **43** (2012) 555; arXiv:1111.7080.
- [23] J. Adams *et al.* (STAR Collaboration) Phys. Rev. C **72** (2005) 014904.
- [24] S. Voloshin and Y. Zhang, Z. Phys. C **70** (1996) 665.
- [25] A. M. Poskanzer and S. A. Voloshin, Phys. Rev. C **58** (1998) 1671.
- [26] S. S. Adler *et al.* (PHENIX Collaboration), Phys. Rev. Lett. **91** (2003) 182301.
- [27] S. A. Voloshin, A. M. Poskanzer, R. Snellings, arXiv:0809.2949.
- [28] N. Borghini, P. M. Dinh, J. Y. Ollitrault, Phys. Rev. C **64** (2001) 054901.
- [29] K. Aamodt *et al.* (ALICE Collaboration), Phys. Rev. Lett. **105** (2010) 252302.
- [30] Z. T. Yang, W. N. Zhang, L. Huo, J. B. Zhang, J. Phys. G. **36** (2009) 015133.
- [31] C. Y. Wong, W. N. Zhang, Phys. Rev. C **70** (2004) 064904.
- [32] W. N. Zhang, Shu-Xia Li, C. Y. Wong, M. J. Efaaf, Phys. Rev. C **71** (2005) 064908.
- [33] Hu Ying, Su Zhongqian, Zhang Weining, Nuclear Science and Techniques **24** (2013) 050522.
- [34] G. Bertsch, M. Gong, M. Tohyama, Phys. Rev. C **37** (1988) 1896; G. Bertsch, Nucl. Phys. A **498** (1989) 173c.
- [35] S. Pratt, T. Csörgo, and J. Zimányi, Phys. Rev. C **42** (1990) 2646.